ELSEVIER

Journal of Fluids and Structures 24 (2008) 1349–1357

JOURNAL OF FLUIDS AND STRUCTURES

www.elsevier.com/locate/jfs

Active control of flow separation over an airfoil using synthetic jets

D. You*, P. Moin

Center for Turbulence Research, Stanford University, Stanford, CA 94305, USA

Received 29 January 2008; accepted 21 June 2008
Available online 31 October 2008

Abstract

We perform large-eddy simulation of turbulent flow separation over an airfoil and evaluate the effectiveness of synthetic jets as a separation control technique. The flow configuration consists of flow over an NACA 0015 airfoil at Reynolds number of 896,000 based on the airfoil chord length and freestream velocity. A small slot across the entire span connected to a cavity inside the airfoil is employed to produce oscillatory synthetic jets. Detailed flow structures inside the synthetic-jet actuator and the synthetic-jet/cross-flow interaction are simulated using an unstructured-grid finite-volume large-eddy simulation solver. Simulation results are compared with the 2005 experimental data of Gilarranz et al., and qualitative and quantitative agreements are obtained for both uncontrolled and controlled cases. As in the experiment, the present large-eddy simulation confirms that synthetic-jet actuation effectively delays the onset of flow separation and causes a significant increase in the lift coefficient. Modification of the blade boundary layer due to oscillatory blowing and suction and its role in separation control is discussed.

Keywords: Separation control; Synthetic jets; Large-eddy simulation

1. Introduction

The performance of an airplane wing has a significant impact on the runway distance, approach speed, climb rate, payload capacity, and operation range, but also on the community noise and emission level as an efficient lift system also reduces thrust requirements [e.g., Thibert et al. (1995)]. The performance of an airplane wing is often degraded by flow separation. Flow separation on an airfoil surface is related to the aerodynamic design of the airfoil profile. However, non-aerodynamic constraints such as material property, manufacturability, and stealth capability in military applications often conflict with the aerodynamic constraints, and either passive or active flow control is required to overcome the difficulty. Passive control devices, for example, vortex generators (Jirasek, 2004), have proven to be effective in delaying flow separation under some conditions. However, they can introduce a drag penalty when the flow does not separate. Over the past several decades various active flow control concepts have been proposed and evaluated to improve the efficiency and stability of lift systems by controlling flow separation. Many of these techniques involve continuous blowing or suction, which can produce effective control but is difficult to apply in real applications.

*Corresponding author. Tel.: +1 650 725 1821; fax: +1 650 725 3525.
E-mail address: dyou@stanford.edu (D. You).

0889-9746/$ - see front matter © 2008 Elsevier Ltd. All rights reserved.
doi:10.1016/j.jfluidstructs.2008.06.017

In recent years, control devices involving zero-net-mass-flux oscillatory jets or synthetic jets have shown good feasibility for industrial applications and effectiveness in controlling flow separation [e.g., Glezer and Amitay (2002), Rumsey et al. (2004), Wygnanski (2004), Findanis and Ahmed (2008)]. The application of synthetic jets to flow separation control is based on their ability to stabilize the boundary layer by adding/removing momentum to/from the boundary layer with the formation of vortical structures. The vortical structures in turn promote boundary layer mixing and hence momentum exchange between the outer and inner parts of the boundary layer. The control performance of the synthetic jets greatly relies on parameters such as the amplitude, frequency, and location of the actuation. Therefore an extensive parametric study is necessary for optimizing the control parameters.

For numerical simulations, an accurate prediction, not to mention control, of the flow over an airfoil at practical Reynolds numbers is a challenging task. The flow over an airfoil is inherently complex and exhibits a variety of physical phenomena including strong pressure gradients, flow separation, and confluence of boundary layers and wakes [e.g., Khorrami et al. (1999, 2000), Ying et al. (1998), Mathias et al. (1999)]. The complex unsteady flow is difficult to compute by traditional computational fluid dynamics (CFD) techniques based on Reynolds-averaged Navier–Stokes (RANS) equations (Rumsey and Ying, 2002). For prediction of such unsteady flows, large-eddy simulation (LES) offers the best promise in the foreseeable future because it provides detailed spatial and temporal information regarding a wide range of turbulence scales, which is precisely what is needed to gain better insight into the flow physics of this configuration.

Recently, Gilarranz et al. (2005) performed an experimental study of flow separation over an NACA 0015 airfoil with synthetic-jet control. They reported the flow visualization, mean pressure coefficients, and wake profiles in both controlled and uncontrolled cases. However, the mechanism for separation control and how the boundary layer is modified by the control have not been clearly identified. In the present study we address the issues using LES. An understanding of the control mechanisms is valuable in reducing the effort for optimizing the control parameters.

In this study we employ an unstructured-grid LES solver, CDP (Ham and Iaccarino, 2004), to predict turbulent flow separation over an airfoil and its control by synthetic jets, and to understand the control mechanism for separation control. The unstructured-grid capability of the solver allows us to effectively handle the complex flow configuration involving an embedded synthetic-jet actuator and wind-tunnel walls. In Section 2, the computational methodology including a brief introduction of the numerical method, flow configuration, and other computational parameters used for the present LES are described. The present LES results are compared to the experimental data (Gilarranz et al., 2005) in both controlled and uncontrolled cases, and the effects of flow control on the boundary layer properties, flow separation, and lift enhancement are discussed in Section 3, followed by concluding remarks in Section 4.

2. Computational methodology

2.1. Numerical method

The numerical algorithm and solution methods are described in detail by Ham and Iaccarino (2004); the main features of the methodology are summarized here. The spatially filtered incompressible Navier–Stokes equations for resolved scales in LES are

$$\frac{\partial \overline{u}_i}{\partial t}+\frac{\partial}{\partial x_j}\overline{u}_i\overline{u}_j=-\frac{\partial \overline{p}}{\partial x_i}+\frac{1}{\mathrm{Re}}\frac{\partial}{\partial x_j}\frac{\partial \overline{u}_i}{\partial x_j}-\frac{\partial \tau_{ij}}{\partial x_j}, \tag{1}$$

$$\frac{\partial \overline{u}_i}{\partial x_i}=0, \tag{2}$$

where τ_{ij} is the subgrid-scale (SGS) stress tensor modeled either by the dynamic Smagorinsky closure (Germano et al., 1991) or the dynamic global-coefficient model (You and Moin, 2007). In the present LES, the two different SGS models are found to predict similar results. All the coordinate variables, velocity components, and pressure are non-dimensionalized by the airfoil chord length C, the inflow freestream velocity U_∞, and ρU_∞^2, respectively. The time is normalized by C/U_∞. The Cartesian velocity components and pressure are stored at the center of the computational elements. A numerical method that emphasizes discrete kinetic energy conservation was developed for the above equations on unstructured grids with hybrid, arbitrary elements. Controlling aliasing errors using kinetic energy conservation instead of employing numerical dissipation or filtering has been shown to provide good predictive capability for successful LES (You et al., 2006).

The temporal integration method used to solve the governing equations is based on a fully implicit fractional-step method that avoids the severe time-step restriction that would occur in the synthetic-jet orifice region with an explicit scheme. All terms in Eqs. (1) and (2) are advanced using a second-order accurate fully implicit method in time, and are discretized by the second-order central difference in space. A bi-conjugate gradient stabilized method (BCGSTAB) is used to solve the discretized nonlinear equations. The Poisson equation is solved by an algebraic multigrid method.

2.2. Flow configuration

The flow configuration is shown in Fig. 1. This configuration was experimentally studied by Gilarranz et al. (2005). In the experiment, an NACA 0015 airfoil with a chord length of 375 mm was installed in a wind tunnel. The slot of the actuator had a width of 2 mm across the entire length of the span and was placed at 12% of the chord measured from the leading edge on the suction side of the airfoil. This location was selected to provide sufficient volume to accommodate the synthetic-jet actuator inside the airfoil.

Fig. 2 shows the maximum lift coefficient measured in the experiment (Gilarranz et al., 2005) as a function of angle of attack (α) in both the uncontrolled and controlled cases. The use of the synthetic-jet actuator causes a dramatic increase in the maximum lift coefficient when the baseline (uncontrolled) flow separates. In the experiment, it was found that the angle of attack for which stall occurs is increased from 12° for an uncontrolled airfoil to approximately 18° for the controlled case. For the synthetic-jet actuation, the frequency of the actuation in the range of 60–130 Hz (or $fC/U_\infty = 0.65-1.40$) does not seem to have a significant effect on the maximum lift coefficient. Fig. 2 indicates that the uncontrolled airfoil first suffers from a docile stall, which is also referred to as a trailing-edge stall when the angle of attack reaches approximately 12°. The separation point gradually moves upstream as the angle of attack increases. The leading-edge stall at approximately 19° produces an abrupt change in the lift coefficient. With the synthetic-jet actuation, the docile stall is effectively controlled and produces further enhanced lift coefficient up to the attack angle of approximately 18°. For an angle of attack greater than 18°, the controlled airfoil also suffers from a

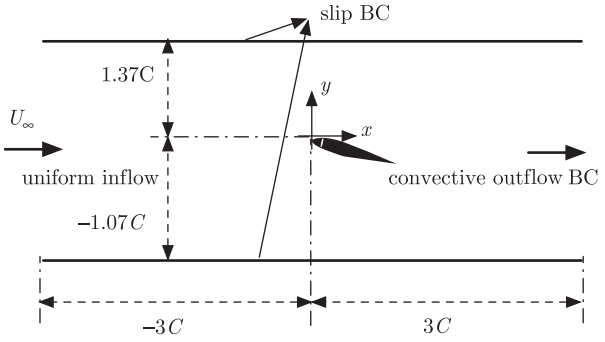

Fig. 1. Flow configuration for LES of flow over an NACA 0015 airfoil with synthetic-jet control.

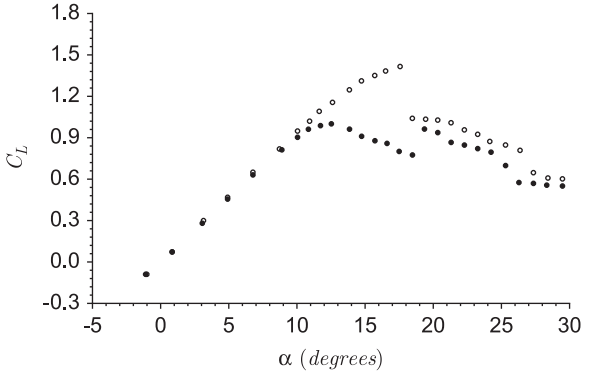

Fig. 2. Lift coefficient as a function of angle of attack (α) measured by Gilarranz et al. (2005): ○, controlled case ($f = 1.2U_\infty/C$); •, uncontrolled case.

sharp drop of the lift coefficient due to the leading-edge stall, which is characterized by the formation of a separation bubble near the leading edge. Even after the massive stall (leading-edge stall) occurs, the synthetic-jet actuation increases the maximum lift coefficient compared to the uncontrolled case, but the amount of the lift augmentation is relatively small.

The present study focuses on the case with the angle of attack of 16.6°, where flow separates from the mid-chord location of the airfoil in the uncontrolled case, and the control effect is most remarkable. For this angle of attack, experimental data such as the mean surface pressure coefficients and wake profiles are available for comparison (Gilarranz et al., 2005). The computational domain is of size $L_x \times L_y \times L_z = 6C \times 2.44C \times 0.2C$. In the present LES, a smaller domain size than that in the experiment is employed in the spanwise direction to reduce the computational cost. The Reynolds number of this flow is 8.96×10^5, based on the airfoil chord and inflow freestream velocity. In this study, it is important to precisely predict the flow through the synthetic-jet actuator because the directional variation of the jets during the oscillatory period greatly affects the boundary layer. Therefore, in the present study, the flow inside the actuator and resulting synthetic jets are simulated along with the external flow field using an unstructured-grid capability of the present LES solver. Fig. 3(a) shows the synthetic-jet actuator modeled with an unstructured mesh. In the experiment, a piston engine is utilized to generate a sinusoidal mass flux and generates synthetic jets through the spanwise cavity slot. To mimic the oscillatory motion of a piston engine in the experiment, we apply sinusoidal velocity boundary conditions to a cavity side wall as shown in Fig. 3(b) and as follows:

$$(u, v, w)_{\text{piston}} = (\cos(\alpha), -\sin(\alpha), 0) A_p \sin(2\pi f t) U_\infty. \tag{3}$$

The frequency of the sinusoidal oscillation of the cavity side wall is $f = 1.284 U_\infty / C$, which corresponds to 120 Hz in the experiment of Gilarranz et al. (2005). A_p corresponds to the amplitude of oscillatory motion of the piston generating the peak bulk jet velocity of $U_{\max} = 2.14 U_\infty$ at the cavity exit nozzle. The same momentum coefficient as in the experiment is produced as

$$C_\mu = \frac{h(\rho U_{\max}^2) \sin\theta_j}{C(\rho U_\infty^2)} = 1.23 \times 10^{-2}, \tag{4}$$

where h and $\theta_j (= 30.2°)$ are the width of the cavity nozzle exit and the jet angle with respect to the airfoil surface. Fig. 3(b) shows the spanwise vorticity contours representing flow inside the cavity and the interaction between synthetic jets and boundary layer flow.

No-stress boundary conditions are applied along the top and bottom of the wind tunnel, and no-slip boundary conditions are applied on the airfoil surface and cavity wall. Periodic boundary conditions are used along the spanwise (z) direction. At the exit boundary, the convective boundary condition is applied, with the convection speed determined by the streamwise velocity averaged across the exit plane.

Two different mesh sizes of approximately 8 and 15 million cells have been employed to examine grid resolution effect on the LES solution. Grid lines are clustered around the nozzle of synthetic-jet actuator, blade boundary layer, and near wake to ensure appropriate resolution in important flow regions. A total of 24 and 30 mesh points are allocated along the cavity slot in the 8- and 15-million-cell meshes, respectively. The 15-million-cell mesh is constructed by refining the 8-million-cell mesh especially in the boundary layer wall-normal direction and spanwise direction. The grid resolution on the blade surface is reasonable compared to other LES studies of wall-bounded turbulent flows using

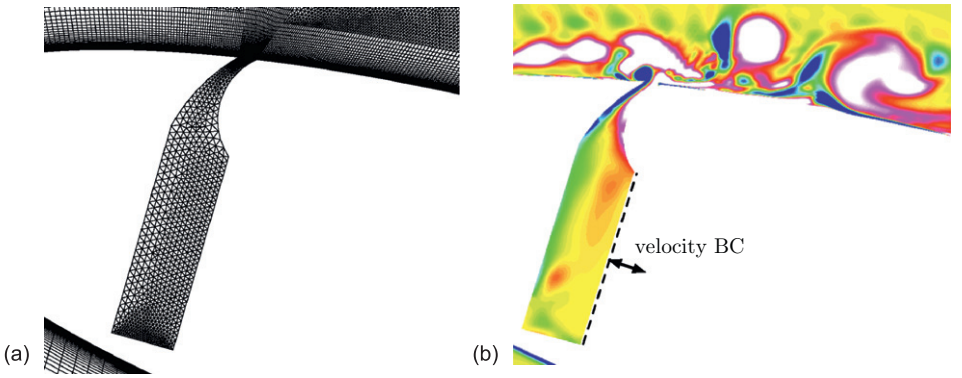

Fig. 3. (a) Computational mesh and (b) instantaneous spanwise vorticity contours inside and around the synthetic-jet actuator. Twenty contour levels in the range of −50 to 60 are shown.

the same solver (You and Moin, 2007). The grid spacings are distributed such that the resolution before the separation is less than 60, 0.5, and 50 wall-units in the streamwise, wall-normal, and spanwise directions, respectively. The simulation is advanced in time with the time step $\Delta t U_\infty/C = 1.7 \times 10^{-4}$ which corresponds to the Courant–Friedrichs–Lewy (CFL) number smaller than 1 in the most of the computational domain except for the region of synthetic-jet nozzle where the CFL number becomes up to 20. When the 15-million-cell mesh is employed, each time step requires a wallclock time of approximately 4.8 s when 200 CPUs of IBM Power5 are used. The present results are obtained by integrating the governing equations over an interval of approximately $20C/U_\infty$.

3. Results and discussion

Gross features of the flow over uncontrolled and controlled airfoils are revealed in Fig. 4, showing iso-surfaces of the instantaneous vorticity magnitude overlapped with pressure contours predicted by the present LES. The vortical structures present over the suction surface qualitatively indicate the degree of flow separation. In the uncontrolled case (Fig. 4(a)), flow massively separates from the half aft portion of the suction surface while the flow separation is dramatically prevented with the synthetic-jet actuation in the controlled case (Fig. 4(b)). Qualitatively, these features are consistent with the change in the experimentally measured maximum lift coefficient (Gilarranz et al., 2005) with flow control (see Fig. 2).

The pressure distributions over the airfoil surfaces in both uncontrolled and controlled cases are compared with the experimental data in Fig. 5. In general, the present LES shows favorable agreement with experimental measurements in both cases. The pressure distribution directly indicates the effect of synthetic jets on flow separation. As seen in Fig. 5, most of the lift enhancement is achieved in the upstream portion of the airfoil suction surface, while the control effect of synthetic jets on the pressure distribution in the pressure surface is negligible.

The lift and drag coefficients predicted by the present LES in the uncontrolled and controlled cases are in excellent agreement with the experimental data (Gilarranz et al., 2005) as shown in Table 1. The present synthetic-jet actuation with the momentum coefficient of 1.23% produces more than a 70% increase in the lift coefficient. The drag coefficient is found to decrease approximately 15–18% with the synthetic-jet actuation.

The drag reduction due to the synthetic-jet actuation is also indicated by the wake profiles. Fig. 6 shows the mean streamwise velocity profiles in the uncontrolled (– – – –) and controlled (——) cases in a downstream location at $x/C = 1.2$. The width of the wake and the peak magnitude of velocity deficit decrease with synthetic-jet control. The present wake profiles are in favorable agreement with experimental data (Gilarranz et al., 2005) in both uncontrolled and controlled cases.

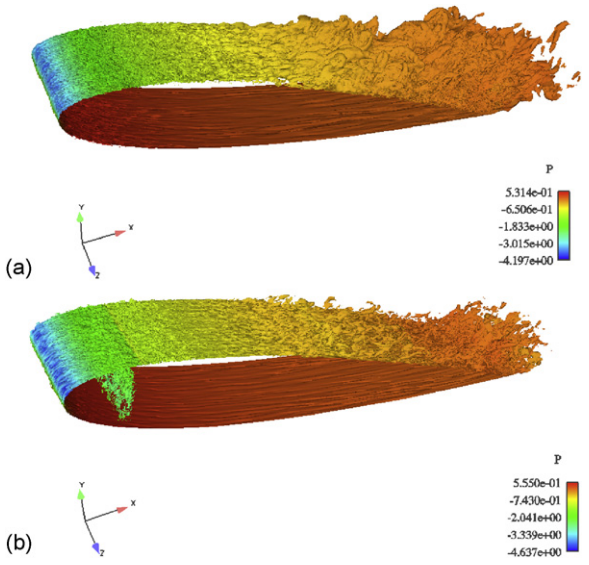

Fig. 4. Iso-surfaces of the instantaneous vorticity magnitude ($|\Omega|C/U_\infty$) of 40 overlapped with the pressure contours: (a) uncontrolled case; (b) controlled case.

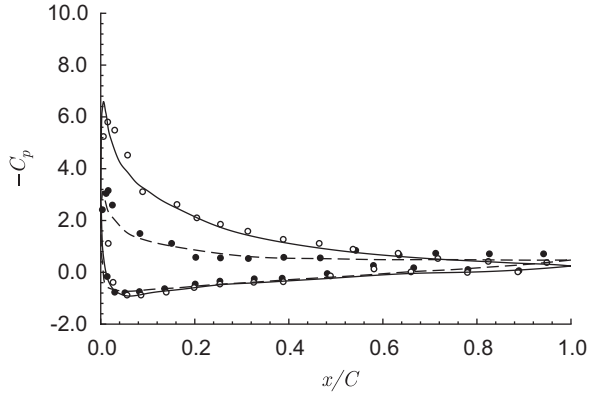

Fig. 5. Mean pressure distribution over the airfoil surface. Solid line, controlled case; dashed line, uncontrolled case; symbols, experimental data (Gilarranz et al., 2005). LES results on the 15-million-cell mesh are shown.

Table 1
Summary of lift and drag coefficients

Case	Uncontrolled		Controlled	
	C_L	C_D	C_L	C_D
Present LES [15-million-cell mesh]	0.81	0.28	1.40	0.22
Experiment (Gilarranz et al., 2005)	0.82	0.26	1.41	0.22

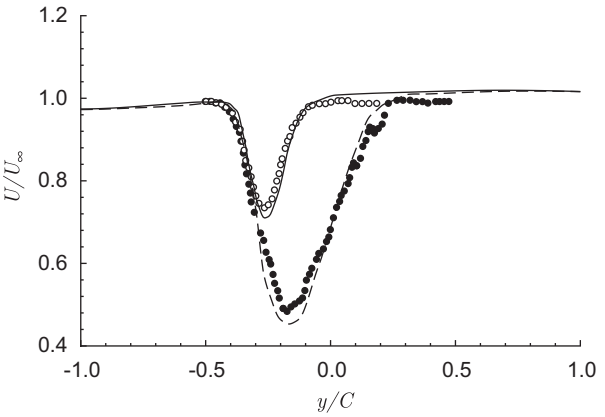

Fig. 6. Mean streamwise velocity profiles at $x/C = 1.2$. Solid line, controlled case; dashed line, uncontrolled case; symbols, experimental data (Gilarranz et al., 2005). LES results on the 15-million-cell mesh are shown.

Both the suction and blowing phases significantly modify the boundary layer on the suction surface of the airfoil. The synthetic-jet actuation not only stabilizes the boundary layer either by adding/removing the momentum to/from the boundary layer, but also enhances mixing between inner and outer parts of the boundary layer. The change of the blade boundary layer during a period of synthetic-jet actuation is shown in Fig. 7 in terms of the phase-averaged streamlines. In the suction phase (Fig. 7(a)) the low momentum flow in the upstream boundary layer is removed by the suction and prevents downstream flow separation. On the other hand, synthetic-jet blowing (Fig. 7(c)) energizes the downstream boundary layer and prevents downstream flow separation. The modification of the boundary layer in the upstream ($x/C = 0.11$) and downstream ($x/C = 0.16$) proximity to the exit slot of the synthetic-jet actuator ($x/C = 0.12$) is shown in Fig. 8. Compared to the velocity profile in the uncontrolled case (○), in the suction phase (Fig. 8(a)), the thickness of the downstream boundary layer is significantly thinned. On the other hand, in the blowing phase

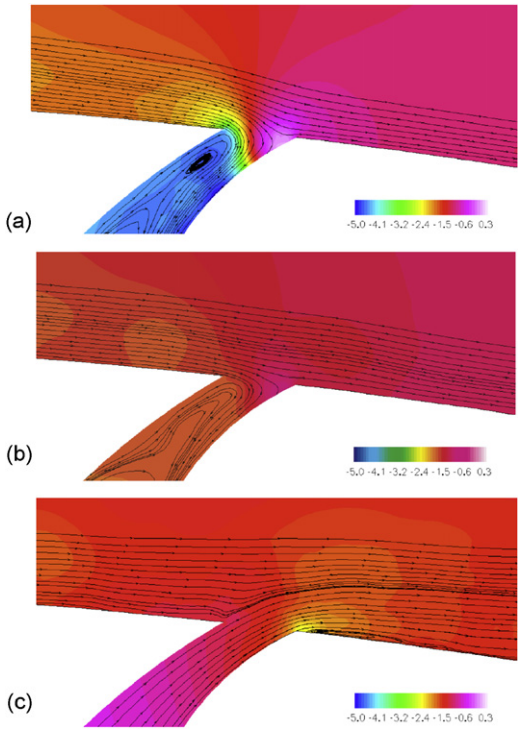

Fig. 7. Mean streamlines overlapped by the mean pressure contours. (a) $(\frac{1}{4})T$ (suction phase); (b) $(\frac{2}{4})T$; (c) $(\frac{3}{4})T$ (blowing phase), where T denotes the period of synthetic-jet actuation.

(Fig. 8(b)), the downstream velocity profile becomes fuller due to additional momentum while the modification of the upstream velocity profile is not noticeable. Therefore, the downstream flow separation is effectively prevented by the favorable modification of the blade boundary layer in both the blowing and suction phases.

The shape factors of the boundary layer which is defined as a ratio of the displacement thickness to the momentum thickness in different control phases are compared to the shape factor of the uncontrolled boundary layer at $x/C = 0.16$ in Fig. 9. In general, a larger shape factor implies that the boundary layer is more prone to separation. As seen in Fig. 9, smaller shape factors compared to that in the uncontrolled cases are observed in most of the control phases. The reduction of the shape factor is especially significant in the suction phases. However, in the blowing phase at $\theta = 337.5°$, the shape factor becomes slightly larger than that of uncontrolled case, and this imply the presence of intermittent separation even in the controlled case.

4. Conclusions

We performed large-eddy simulations (LESs) of turbulent flow separation over an airfoil at a high Reynolds number and investigated the effectiveness of synthetic jets as a separation control technique. Detailed flow structures inside the synthetic-jet actuator and the synthetic-jet/cross-flow interaction were predicted by using an unstructured-grid LES solver. Qualitative and quantitative agreements with experimental data are obtained for both uncontrolled and controlled cases. The present LES confirms the experimental observation (Gilarranz et al., 2005) that synthetic jets which are produced through a slot across the entire span connected to a cavity inside the airfoil, effectively delays the onset of flow separation and causes about 70% increase in the lift coefficient. Both the suction and blowing phases are found to significantly modify the boundary layer on the suction surface of the airfoil. The synthetic-jet actuation not only stabilizes the boundary layer either by adding/removing the momentum to/from the boundary layer, but also enhances mixing between inner and outer parts of the boundary layer. In the suction phase the low momentum flow in the boundary layer is removed by the suction and prevents downstream flow separation. On the other hand, synthetic-jet blowing energizes the downstream boundary layer and prevents downstream flow separation.

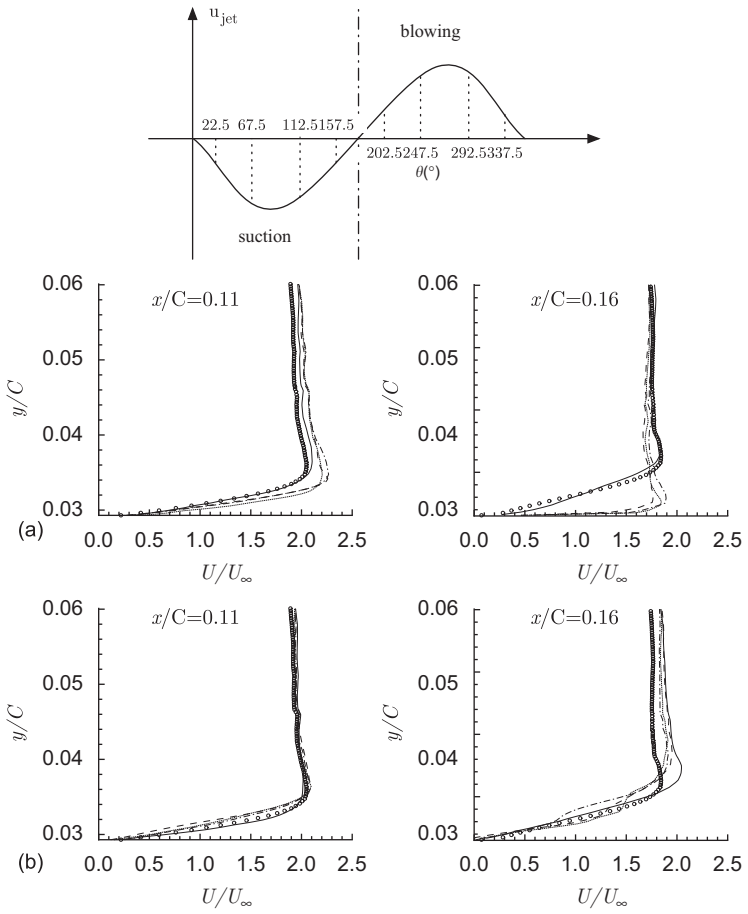

Fig. 8. Profiles of the phase-averaged streamwise velocity. (a) Suction phase: ——, $\theta = 22.5^\circ$; – – – –, 67.5°; ·····, 112.5°; —·—, 157.5°; (b) blowing phase: ——, $\theta = 202.5^\circ$; – – – –, 247.5°; ·····, 292.5°; —·—, 337.5°. ○, Uncontrolled case. The cavity slot is located at $x/C = 0.12$.

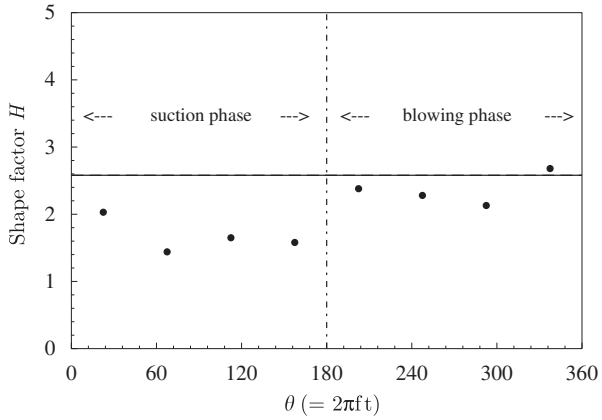

Fig. 9. Shape factor (ratio of the displacement thickness to the momentum thickness) of the boundary layer at $x/C = 0.16$ in different control phases shown in Fig. 8: ——, shape factor in the uncontrolled case (2.58), •, shape factor in the controlled case.

Acknowledgments

The authors gratefully acknowledge support from Boeing company and valuable discussions with Arvin Shmilovich. The authors are also grateful to Frank Ham for his help with the unstructured LES solver CDP.

References

Findanis, N., Ahmed, N.A., 2008. The interaction of an asymmetrical localised synthetic jet on a side-supported sphere. Journal of Fluids and Structures, doi:10.1016/j.fluidstructs.2008.02.002.

Germano, M., Piomelli, U., Moin, P., Cabot, W.H., 1991. A dynamic subgrid-scale eddy-viscosity model. Physics of Fluids (A) 3 (7), 1760–1765.

Gilarranz, J.L., Traub, L.W., Rediniotis, O.K., 2005. A new class of synthetic jet actuators—part II: application to flow separation control. ASME Journal of Fluids Engineering 127, 377–387.

Glezer, A., Amitay, M., 2002. Synthetic jets. Annual Review of Fluid Mechanics 34, 503–529.

Ham, F., Iaccarino, G., 2004. Energy conservation in collocated discretization schemes on unstructured meshes. Annual Research Briefs, Center for Turbulence Research, Stanford, CA, pp. 3–14.

Jirasek, A., 2004. A vortex generator model and its application to flow control. AIAA Paper 2004-4965.

Khorrami, M.R., Singer, B.A., Radeztsky, R.H., 1999. Reynolds-averaged Navier–Stokes computations of a flap-side-edge flowfield. AIAA Journal 37 (1), 14–22.

Khorrami, M.R., Berkman, M.E., Choudhari, M., 2000. Unsteady flow computations of a slat with blunt trailing edge. AIAA Journal 38 (11), 2050–2058.

Mathias, D.L., Roth, K.R., Ross, J.C., Rogers, S.E., Cummings, R.M., 1999. Navier–Stokes analysis of the flow about a flap edge. Journal of Aircraft 36 (6), 833–838.

Rumsey, C.L., Ying, S.X., 2002. Prediction of high lift: review of present CFD capability. Progress in Aerospace Sciences 38, 145–180.

Rumsey, C.L., Gatski, T.B., Sellers III, W.L., Vatsa, V.N., Viken, S.A., 2004. Summary of the 2004 CFD validation workshop on synthetic jets and turbulent separation control. AIAA Paper 2004-2217.

Thibert, J.J., Reneaux, J., Moens, F., Priest, J., 1995. ONERA activities on high lift devices for transport aircraft. Aeronautical Journal 99, 395–411.

Wygnanski, I., 2004. The variables affecting the control of separation by periodic excitation. AIAA Paper 2004-2505.

Ying, S.X., Spaid, F.W., McGinley, C.B., Rumsey, C.L., 1998. Investigation of confluent boundary layers in high-lift flows. Journal of Aircraft 35 (3), 550–562.

You, D., Moin, P., 2007. A dynamic global-coefficient subgrid-scale eddy-viscosity model for large-eddy simulation in complex geometries. Physics of Fluids 19 (6), 065110.

You, D., Wang, M., Moin, P., 2006. Large-eddy simulations of flow over a wall-mounted hump with separation control. AIAA Journal 44 (11), 2571–2577.